Supporting Material

Automated Identification of Subcellular Organelles by Coherent Anti-Stokes Raman Scattering

Samir F. El-Mashtoly,[#,§] Daniel Niedieker,[#,§] Dennis Petersen,[§] Sascha Krauß,[§] Erik Freier,[§] Abdelouahid Maghnouj,[‡] Axel Mosig,[§] Stephan Hahn,[‡] Carsten Kötting,[§] and Klaus Gerwert*[,§]

[§]Department of Biophysics, and [‡]Department of Molecular GI-Oncology, Clinical Research Center, Ruhr-University Bochum, 44780 Bochum, Germany

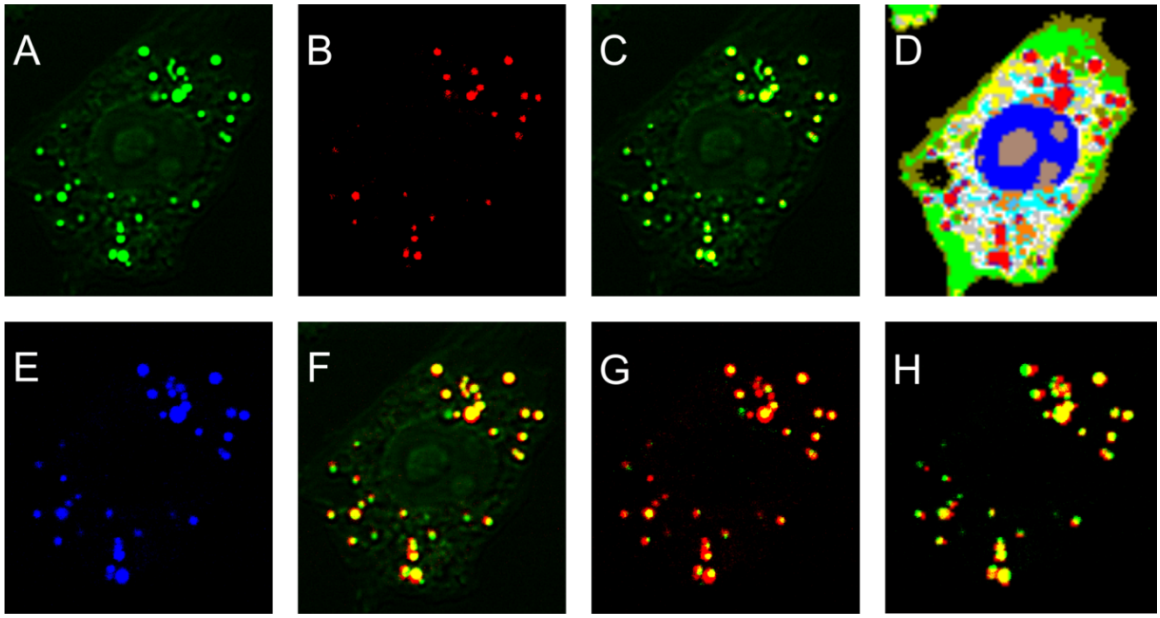

Fig. S1. CARS images were recorded at (A) 2850 cm^{-1} and (B) 1750 cm^{-1}. (C) Overlay of panels (A) and (B). (D) HCA of Raman dataset in the range of 2800-3100 cm^{-1}. (E) Fluorescence image of lipid droplets. (F), (G), and (H) panels display the overlay (A) and (E), (B) and (E), and lipid droplet cluster from (D) and (E) panels, respectively. The overlapped regions are shown in yellow.

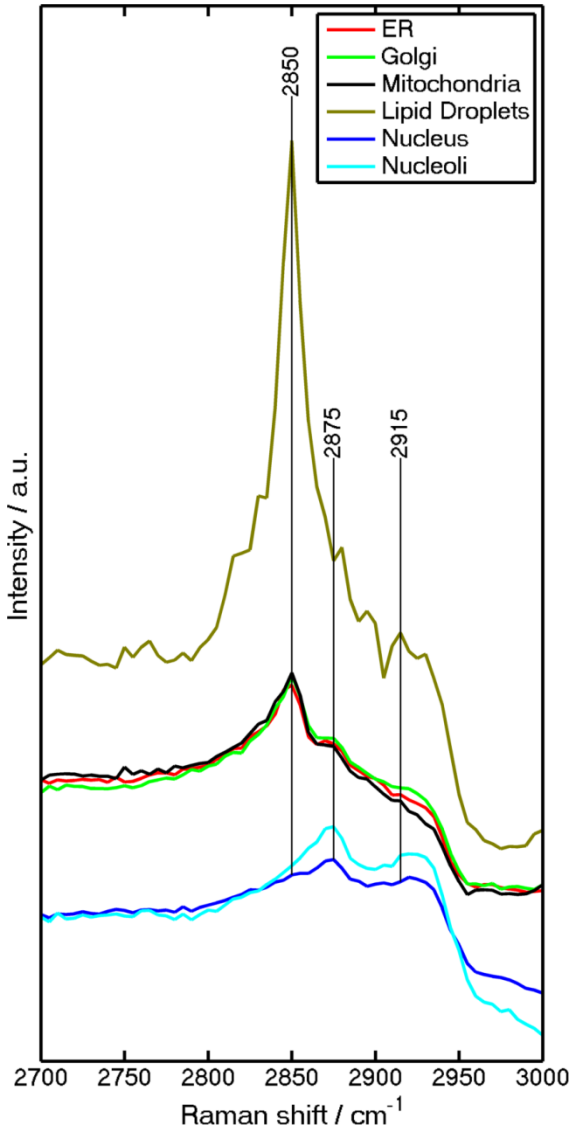

Fig. S2. Mean CARS spectra of subcellular organelles.

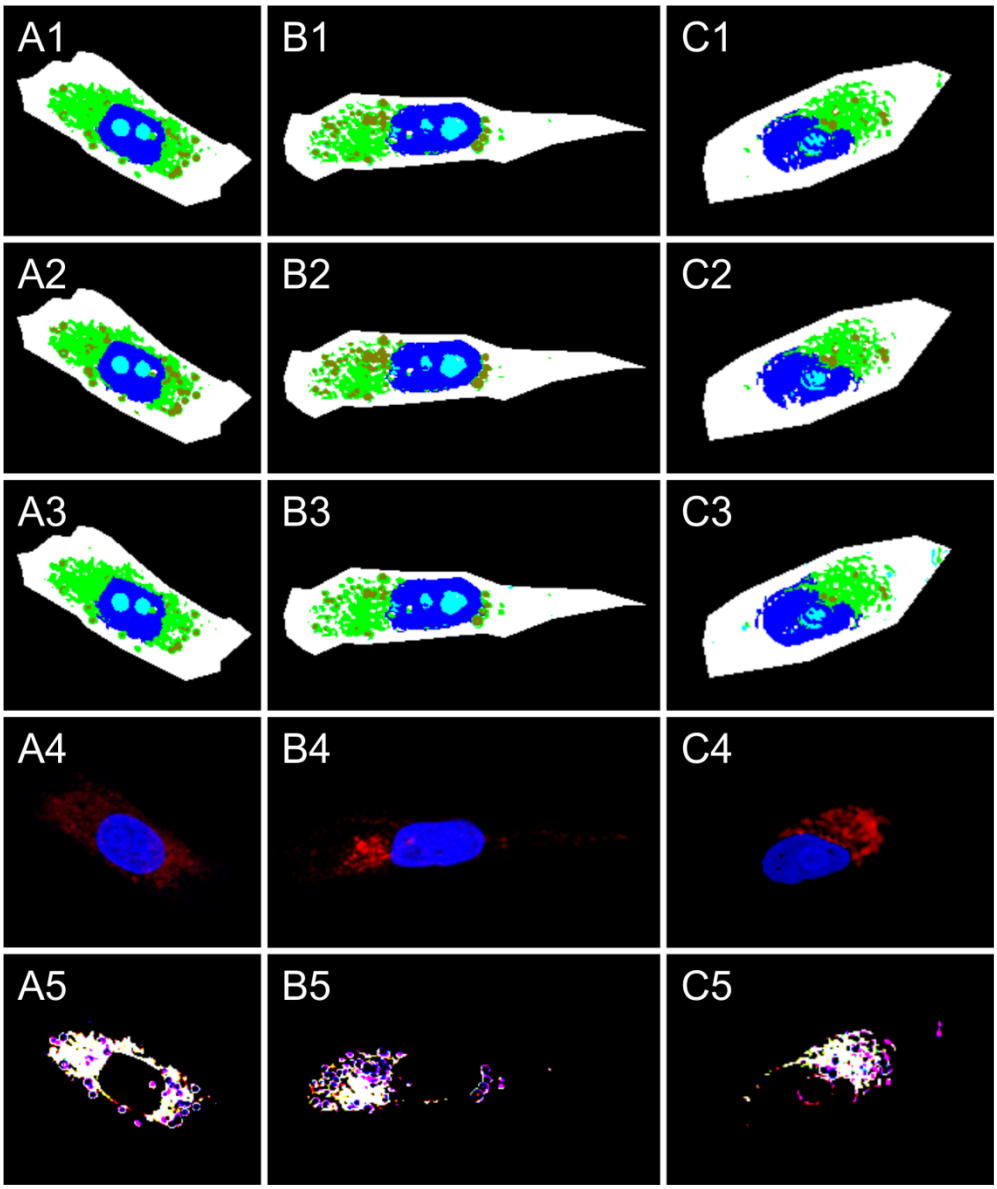

Fig. S3. Automatic identification of the endoplasmic reticulum, Golgi apparatus, and mitochondria. Selective random forests of CARS datasets in which the endoplasmic reticulum (A1-C1), Golgi apparatus (A2-C2), and mitochondria (A3-C3) are displayed in green. (A4-C4) Fluorescence staining (red) of endoplasmic reticulum (A4), Golgi apparatus (B4), and mitochondria (C4) in addition to the nucleus staining (blue). (A5-C5) Overlaid images of random forest classes of endoplasmic reticulum, Golgi apparatus, and mitochondria and the overlapping regions of the three organelles are shown in white.

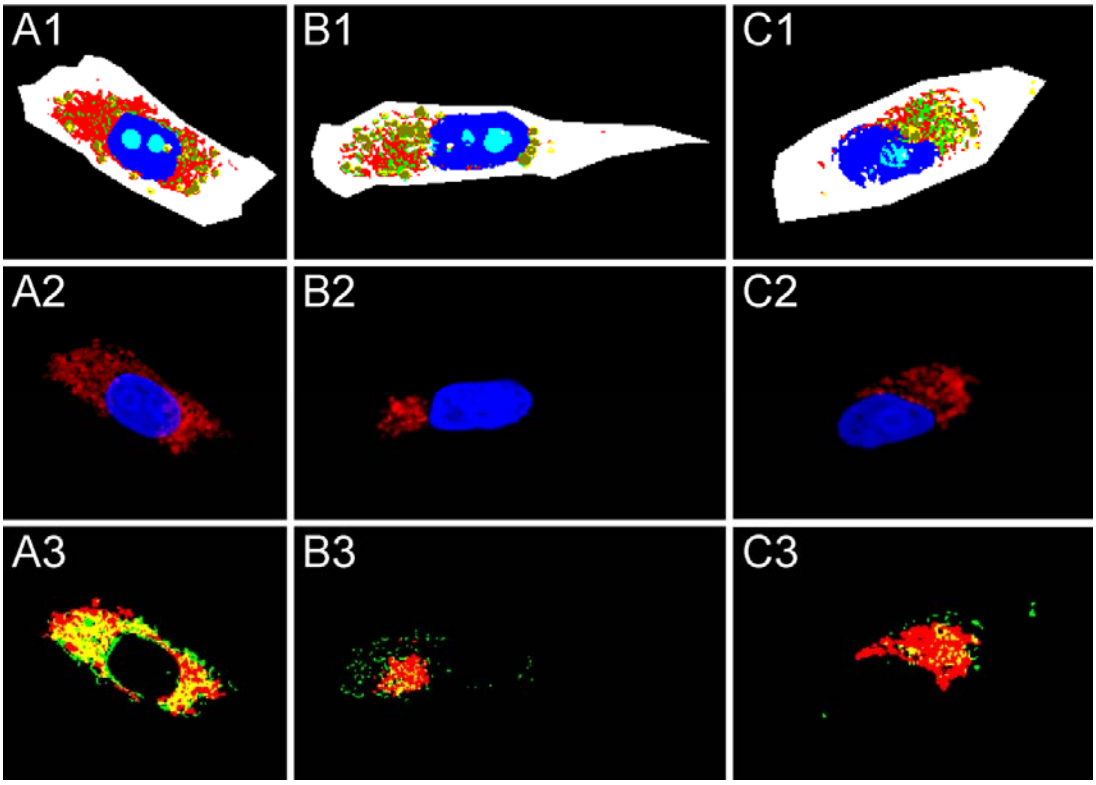

Fig. S4. Simultaneous automatic identification of the endoplasmic reticulum, Golgi apparatus, and mitochondria. (A1-C1) random forest of CARS datasets. (A2-C2) Fluorescence images of the nucleus (blue), endoplasmic reticulum (A2), Golgi apparatus (B2), and mitochondria (C2). (A3-C3) Overlaid images of endoplasmic reticulum, Golgi apparatus, and mitochondria fluorescence (red) from (A2-C2) with their corresponding random forest (green) from (A1-C1) and the overlapping regions are shown in yellow.

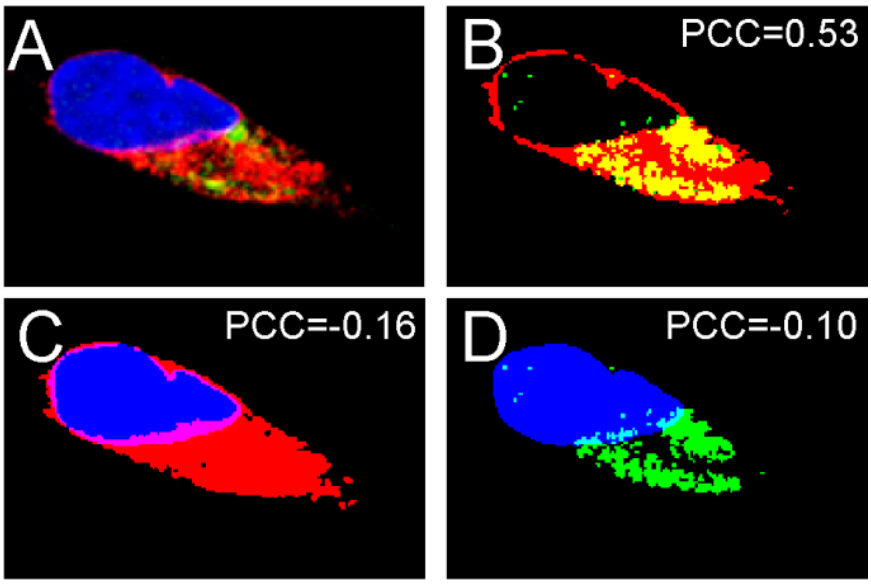

Fig. S5. Colocalization of endoplasmic reticulum and Golgi apparatus. (A) Fluorescence image of nucleus (blue), endoplasmic reticulum (red), and Golgi apparatus (green). The overlay of endoplasmic reticulum and Golgi apparatus (B), endoplasmic reticulum and nucleus (C), and Golgi apparatus and the nucleus (D) are also shown. The overlaid regions are shown in yellow (B), purple (C) and cyan (D).

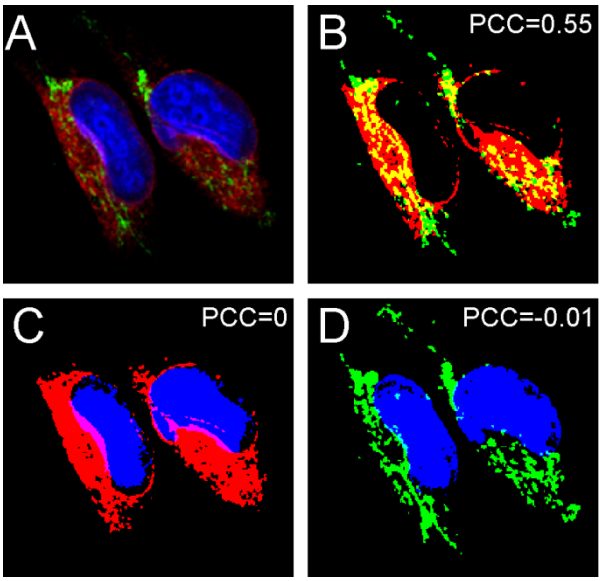

Fig. S6. Colocalization of endoplasmic reticulum and mitochondria. (A) Fluorescence image of nucleus (blue), endoplasmic reticulum (red), and mitochondria (green). The overlay of endoplasmic reticulum and mitochondria (B), endoplasmic reticulum and nucleus (C), and mitochondria and the nucleus (D) are also shown. The overlaid regions are shown in yellow (B), purple (C) and cyan (D).

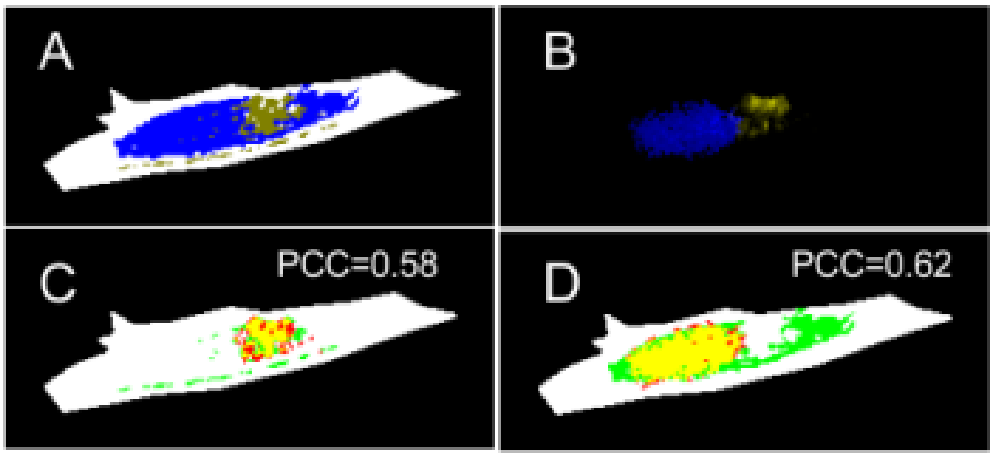

Fig. S7. Automatic identification of the nucleus and lipid droplets in the living cell. (A) Random forest of CARS dataset of the MIA PaCa-2 cell. (B) Fluorescence imaging of the nucleus (blue) and lipid droplets (olive) of the living MIA PaCa-2 cell. Overlaid images of lipid droplets and the nucleus fluorescence (red) from B with their corresponding random forest classes (green) from A are displayed in C (lipid droplets) and D (nucleus), respectively. The overlapping regions are shown in yellow.

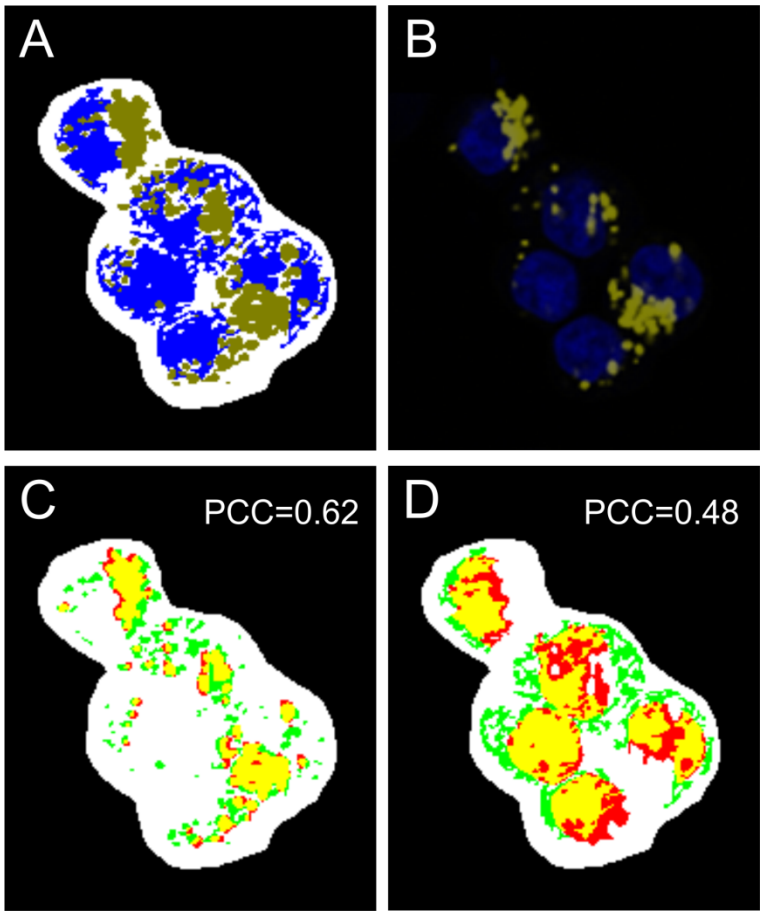

Fig. S8. Automatic identification of the nucleus and lipid droplets of HT29 cells based on a classifier trained on MIA PaCa-2 cells. (A) Random forest of CARS dataset of HT29 cells. (B) Fluorescence imaging of the nucleus (blue) and lipid droplets (olive) of HT29 cells. Overlaid images of lipid droplets and the nucleus fluorescence (red) from B with their corresponding random forest classes (green) from A are displayed in C (lipid droplets) and D (nucleus), respectively. The overlapping regions are shown in yellow.